International Journal of Minerals, Metallurgy and Materials
Volume 18, Number 6, Dec 2011, Page 671
DOI: 10.1007/s12613-011-0494-x

Identification of thermal effects involved in DSC experiment on Al-Cu-Mg-Ag alloys with high Cu:Mg ratio

Jian-bo Zhang, Yong-an Zhang, Bao-hong Zhu, Feng Wang, Zhi-hui Li, Xi-wu Li, and Bai-qing Xiong

State Key Laboratory of Nonferrous Metals and Processes, General Research Institute for Non-ferrous Metals, Beijing 100088, China
(Received: 13 December 2010; revised: 9 January 2011; accepted: 18 January 2011)

Abstract: Precipitation reactions in the differential scanning calorimetry (DSC) of an Al-Cu-Mg-Ag alloy were identified by analyzing the results from hardness test, electrical conductivity test, and transmission electron microscope (TEM) examination. It is discovered that thermal effects can be identified through selected area electron diffraction and bright-field images. The reaction peaks around 171, 231, and 276°C can be attributed to a structural rearrangement of coherent zones, to the precipitation of Ω phases, and to the precipitation of Ω and θ′ and possible combination with the transition of θ′→θ, respectively. In addition, the hardness and electrical conductivity of the alloy change proportionately with the progression of reactions during the heating process. This phenomenon can be attributed to the evolution of the microstructure.

Keywords: aluminum alloys; thermal effects; identification; differential scanning calorimetry; microstructure

1. Introduction

The Al-Cu-Mg-Ag alloy, as a heat-treatable material, exhibits certain excellent properties, such as high strength and good creep resistance. With the excellent thermal stability, these alloys are considered to be candidate materials for future applications in the aerospace industry. The addition of trace amounts of Ag to the Al-Cu-Mg alloys with a high Cu:Mg ratio changes their precipitation behaviour and allows uniform distribution of their beneficial properties. Therefore, understanding of the precipitation behaviour of the alloy during the ageing treatment is necessary.

Differential scanning calorimetry (DSC) is extensively employed for the study of precipitation in Al-based alloys following heat treatment [1]. There are several reports in the published literature detailing the research, including qualitative and quantitative analyses, undertaken to analyse the precipitation properties in the ageing process for aluminum alloys. Starink [1] undertook an excellent application of the DSC in the analysis of reactions and reaction kinetics in Al-based alloys. He emphasised that attention should, first, be focussed on identification of the reaction and phases involved in a DSC experiment prior to their further application. The reactions and phases would, in general, be identified by applying microcosmic analysis methods, including atom probe analysis, high-resolution transmission electron microscopy (HREM), and transmission electron microscopy (TEM) with selected area electron diffraction (SAED). Several such studies have been reported in Refs. [2-5]. In addition, Li and Shenoy [6] reported the results of their study of the reactions in the DSC experiment for an Al-Cu-Mg-Ag alloy with a low Cu:Mg ratio. The types of precipitates in the Al-Cu-Mg series alloys were significantly influenced by the Cu:Mg ratio [7]. Therefore, a study of reactions in the DSC experiment of this alloy with a high Cu:Mg ratio is necessary to extend our understanding of the effect of Ag addition to this alloy.

Considering differences in reactions of Al-Cu-Mg-Ag alloys with low and high Cu:Mg ratios, it becomes necessary to identify phases causing the thermal effects involved in DSC experiment; this information can provide a basis for further application of these and similar alloys. In this study, hardness test, electrical conductivity test, and TEM examination were combined to analyse the reactions and phases in

Corresponding author: Jian-bo Zhang E-mail: zhang4318@163.com

a DSC experiment of an Al-Cu-Mg-Ag alloy with high Cu:Mg ratio.

2. Experimental data

The Al-Cu-Mg-Ag alloy was provided in the form of a 25-mm sheet and its composition is listed in Table 1. The sheet was produced by processes of casting, homogenisation, and extrusion. The solution treatment was performed at 520°C for 2 h and followed by quenching in cold water. The heating-up process was subsequently carried out at a rate of approximately 10°C/min, which simulates the process in the DSC experiment. These samples were quenched in cold water at the start, end, and intermediate stages of the exothermal effect. The temperature was measured by using a temperature-acquisition system of YOKOGAWA MX100.

Table 1. Composition of the alloy wt%

Cu	Mg	Ag	Fe	Si	Ti	Al
4.80-4.90	0.43-0.47	0.34-0.39	≤0.01	≤0.01	≤0.1	Bal.

Note: the DSC measurements were performed on Q100DSC at a constant rate of 10°C/min at 45-400°C.

The TEM observations were performed on a JEM-2010 transmission electron microscope operated at an acceleration voltage of 200 kV. The disc for TEM was mechanically thinned down to 50 μm and then electropolished by using a twinjet machine employing a 25vol% nitric acid solution in methanol at −30°C and in the range of 15 to 20 V.

Samples for hardness and electrical conductivity measurements were cut from the same metal sheet prepared for the DSC experiment. Hardness measurements were carried out on the 430SVD digital Vickers hardness equipment, and the electric conductivity was evaluated by a direct reading type conductivity meter.

3. Results and discussion

3.1. DSC

Fig. 1 presents the DSC trace of the Al-Cu-Mg-Ag alloy after solution and quenching treatments. Three exothermal peaks marked by I, II, and III are apparent in the DSC thermogram. This indicates that three different reactions occur during the heating process. The peak temperatures corresponding to the recorded exothermic effects are 171, 230, and 276°C, respectively.

3.2. Heating-up curves

To identify the phase transformation unambiguously, a sample should be heated to a condition that corresponds with the start of the thermal effect; another sample should be heated to the condition that corresponds with the end of the thermal effect [1]. Therefore, four samples with different codes of A, B, C, and D were treated by the specified protocol listed in Table 2. The heating-up and linear fit curves obtained are depicted in Fig. 2. This indicates that the heating-up rate is less than 10°C/min for all samples tested.

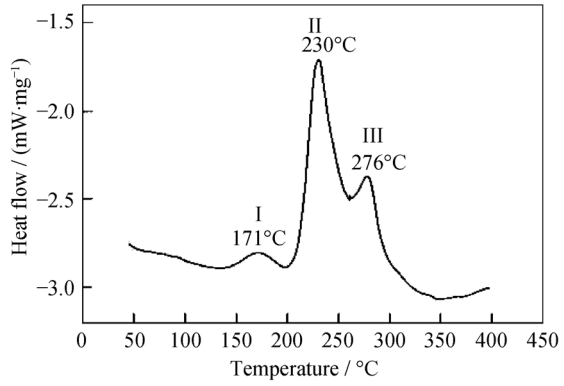

Fig. 1. DSC curve of solution and quenched Al-Cu-Mg-Ag alloy.

Table 2. Parameters of heating-up and quenching

Sample	Heating / (°C·min^{-1})	Quenching / °C
A	9.17	168
B	9.12	232
C	9.00	276
D	9.48	330

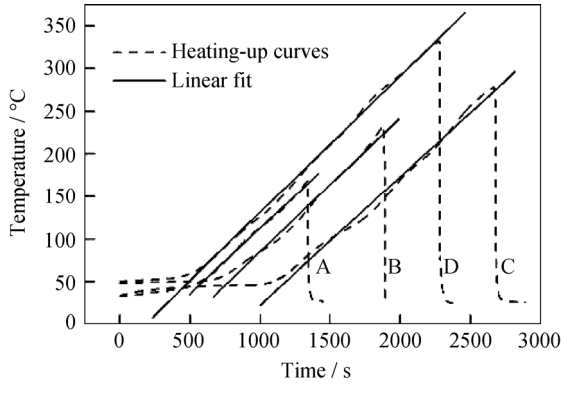

Fig. 2. Heating-up and quenched curves of samples with their linear fit curves.

3.3. Hardness and electrical conductivity

The hardness and electrical conductivity of the tested samples are presented in Fig. 3. The change of the two parameters indicates the evolution of the microstructure, which is investigated by using TEM and is described in the following section. The hardness indicates an increasing trend

with slight fluctuation, whereas the electrical conductivity decreases at the beginning and increases continuously during the heating-up process. These phenomena are explained by the corresponding change in microstructure.

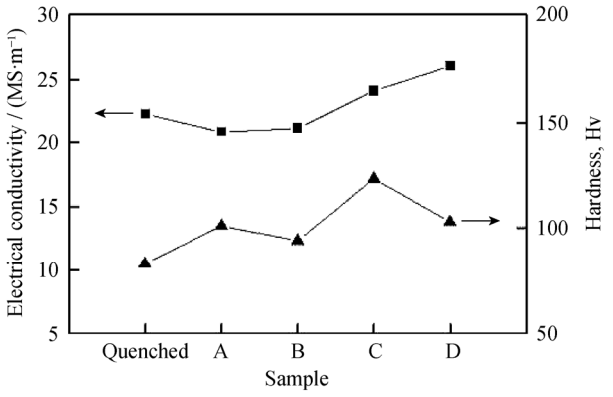

Fig. 3. Hardness and electrical conductivity of samples treated at different conditions.

3.4. TEM

Fig. 4 presents SAED and the corresponding BF image of sample A. Weak streaks are present in the SAED, and this indicates the existence of GP zones in the {100} of the matrix [8]. No obvious diffraction spot of precipitates is observed. Fig. 4(b) reveals that no visible precipitates are present in the microstructure. In addition, the electrical conductivity of this sample is less than that of other quenched sample shown in Fig. 3.

This indicates that the precipitation correlates with the microstructure of the dominant matrix in this condition. From the report presented in Ref. [9], it can be inferred that the exothermic evolution occurred with a broad maximum at approximately 150°C is possibly related to a structural rearrangement of coherent zones.

Fig. 5 shows SAED and BF images for sample B. This sample retains a microstructure that corresponds with the intermediate stage of the exothermal peak II. Two streaks along $[111]_\alpha$ are observed in Fig. 5(a), and there are no obvious streaks in Fig. 5(b). The BF image recorded near $[110]_\alpha$ corresponds with Fig. 5(a) and is depicted in Fig. 5(c). The image indicates that the microstructure is composed of a dense and uniform distribution of precipitates. The characteristics of SAED and BF are consistent with that of the Ω phase reported in Refs. [8-10]. It is concluded that the precipitation of Ω is involved in the thermal effect II. Previously, studies have reported that the Ω phase, with a face-centred orthorhombic structure [7, 11-12] and a chemical composition similar to that of $CuAl_2$, exists as a hexagonal plate-like precipitate in the matrix $\{111\}_\alpha$ planes. Ref. [13] reported that precipitates on the $\{111\}_\alpha$ planes could per-

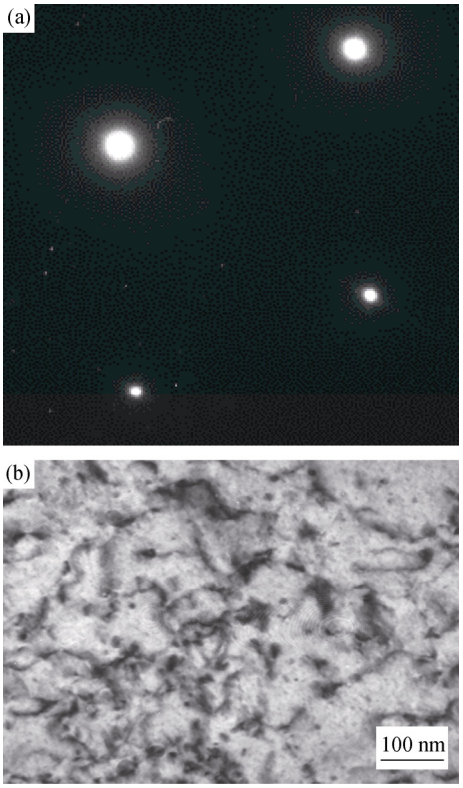

Fig. 4. SAED (a) for zone axis <110> of the matrix and corresponding BF (b) of a sample A.

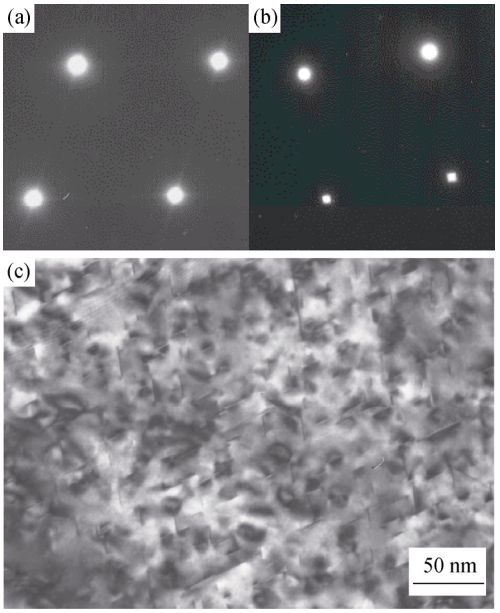

Fig. 5. SAED and BF of sample B: (a) SAED for zone axis <110$_\alpha$>; (b) SAED for zone axis <100$_\alpha$>; (c) BF corresponding to (a).

form more effectively with regard to strength than those on the {100}α planes. However, Fig. 3 indicates that the hardness of the sample that corresponds with the exothermal effect II is less than those of the other samples for the exothermal effect. This conflicts with the discussion reported above. Nevertheless, it can be explained by the instability of GP zones that dissolve by further heating from the temperature of the thermal effect I to that of thermal effect II. By taking into consideration the dissolution temperature and the heat released by the dissolution of GP zones, it can be concluded that the thermal effect II can primarily be attributed to the precipitation of the Ω phase.

Fig. 6 presents SAED and BF images of sample C. In Fig. 6(a), reflections at the l/3 and 2/3 $\{022\}_\alpha$ indicate the presence of the Ω phase, whereas reflections at l/3 and 2/3 $\{\bar{1}10\}_\alpha$ indicate the presence of the θ′ phase [8, 14]. Further confirmation of the presence of Ω and θ′ phases, evidenced by stronger reflections, is also recorded with the electron beam parallel to $[110]_\alpha$, as shown in Fig. 6(b). In addition, pronounced streaks are present in Figs. 6(a) and (b) along different directions. A BF image recorded near $[110]_\alpha$, corresponding with Fig. 6(b), is shown in Fig. 6(c). The microstructure is composed of a dense and uniform distribution of the Ω phase and a small quantity of θ′ nucleating consistently on dislocation. Therefore, the precipitation of both θ′ and Ω can be responsible for the increase in hardness and electrical conductivity.

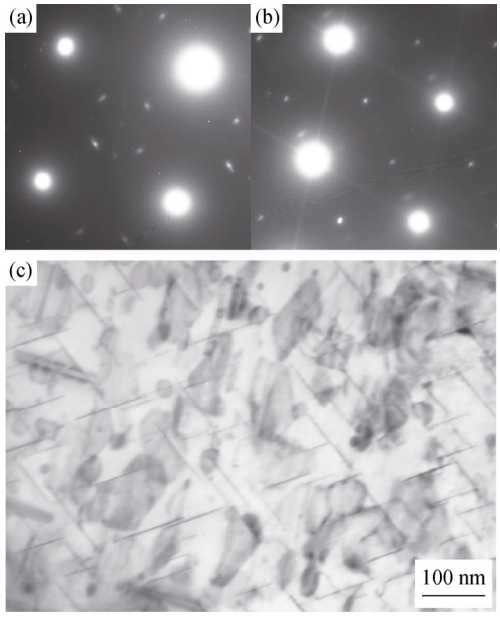

Fig. 6. SAED and BF of sample C: (a) SAED for zone axis $[100]_\alpha$; (b) SAED for zone axis $[110]_\alpha$; (c) BF corresponding to (b).

In comparison with the thermal effect II, it can be concluded that the precipitation of θ′ is involved in the exothermal peak III.

Fig. 7 depicts SAED and BF images of sample D. An observation of Fig. 7(a) and (b) leads to conclude that the characteristics of reflections is consistent with that in Figs. 6(a) and (b). This indicates that both Ω and θ′ phases are present in the microstructure. From Fig. 7(c), a coarsening of Ω and θ′ during the exothermal effect III can be observed. The coarsening of the phases could bring about a decrease in hardness. Careful comparison of the precipitates size in Figs. 6 and 7 indicates that the process of coarsening primarily occurs in the latter part of the thermal effect III. In addition, the thickness of θ′ in Fig. 7(c) is much greater than that of sample C corresponding to the peak of effect III. This indicates that the semi-coherent interface between the matrix and the θ′ can potentially turn into an incoherent interface, and the precipitate θ′ evolves to the stable phase θ. Therefore, the exothermal effect III is mainly attributed to the precipitation of Ω and θ′ phases and possible combination with the transition from θ′ to θ.

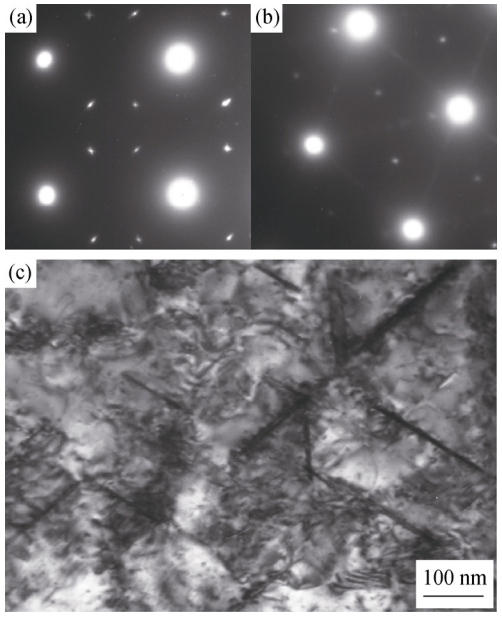

Fig. 7. SAED and BF of the sample D: (a) SAED for zone axis $[100]_\alpha$; (b) SAED for zone axis $[110]_\alpha$; (c) BF corresponding to (b).

4. Conclusion

Three exothermal effects are observed in the DSC experiment of the Al-Cu-Mg-Ag alloy after the treatment of solution and quenching in cold water. The effect peak at approximately 171°C may primarily be attributed to a struc-

tural rearrangement of coherent zones, the effect peak at approximately 231°C is attributed to the precipitation of the Ω phase, and the effect peak at approximately 276°C is attributed to the precipitation of the Ω and θ′ phases and possible combination with the reaction of θ′→θ.

References

[1] M.J. Starink, Analysis of aluminium based alloys by calorimetry: quantitative analysis of reactions and reaction kinetics, *Int. Mater. Rev*., 49(2004), No.3-4, p.3.

[2] J.Y. Yao, D.A. Graham, *et al*., A TEM study of precipitation in Al-Mg-Si alloys, *Micron*, 32(2001), No.8, p.865.

[3] R.D. Sá Lisboa and C.S. Kiminami, Primary crystallization in amorphous $Al_{84}Ni_8Co_4Y_3Zr_1$ alloy, *J. Non Cryst. Solids*, 304(2002), No.1-3, p.36.

[4] S. Abis, M. Massazza, P. Mengucci, and G. Riontino, Early ageing mechanisms in a high-copper AlCuMg alloy, *Scripta Mater.*, 45(2001), No.6, p.685.

[5] Y.J. Li and L. Arnberg, Evolution of eutectic intermetallic particles in DC-cast AA3003 alloy during heating and homogenization, *Mater. Sci. Eng. A*, 347(2003), No.1-2, p.130.

[6] Q. Li and R.N. Shenoy, DSC and TEM characterizations of thermal stability of an Al-Cu-Mg-Ag alloy, *J. Mater. Sci.*, 32(1997), No.13, p.3401.

[7] I.J. Polmear, *Light alloys From Traditional Alloys to Nanocrystals*, Butterworth-Heinemann, Burlington, 2006, p.52,63.

[8] B.M. Gable, G.J. Shiflet, and E.A. Starke, Alloy development for the enhanced stability of Ω precipitates in Al-Cu-Mg-Ag alloys, *Metall. Mater. Trans. A*, 37(2006), No.4 p.1091.

[9] M. Massazza, G. Riontino, A. Dupasquier, *et al.*, Secondary ageing in Al-Cu-Mg, *Philos. Mag. Lett.*, 82(2002), No.9, p.495.

[10] O. Beffort, C. Solenthaler, P.J. Uggowitzer, and M.O. Speidel, High toughness and high strength spray-deposited Al-CuMgAg-base alloys for use at moderately elevated temperatures, *Mater. Sci. Eng. A*, 191(1995), No.1-2, p.121.

[11] S.P. Ringer, T. Sakurai, and I.J. Polmear, Origins of hardening in aged Al-Cu-Mg-(Ag) alloys, *Acta Mater.*, 45(1997), No.9, p.3731.

[12] R.J. Chester and I.J. Polmear, TEM investigation of precipitates in Al-Cu-Mg-Ag and Al-Cu-Mg alloys, *Micron*, 11(1980), No.3-4, p.311.

[13] A.W. Zhu and E.A. Starke Jr, Strengthening effect of unshearable particles of finite size: a computer experimental study, *Acta Mater.*, 47(1999), No.11, p.3263.

[14] S.C. Wang, F. Lefebvre, J.L. Yan, *et al*., VPPA welds of Al-2024 alloys: analysis and modelling of local microstructure and strength, *Mater. Sci. Eng. A*, 431(2006), No.1-2, p.123.